Silicon microring isolator with large optical isolation and low loss

Duanni Huang*,[1], Paolo Pintus[1,2], Chong Zhang[1], Yuya Shoji[3], Tetsuya Mizumoto[4], John E. Bowers[1]

1: Electrical and Computer Engineering Department, University of California Santa Barbara, California 93106, USA
2: Scuola Superiore Sant'Anna, via Moruzzi 1, 56124 Pisa, Italy
3: Quantum Nanoelectronics Research Center, Tokyo Institute of Technology, 2-12-1 Ookayama, Meguro-ku, Tokyo, 152-8552, Japan
4: Department of Electrical and Electronic Engineering, Tokyo Institute of Technology, 2-12-1 Ookayama, Meguro-ku, Tokyo, 152-8552, Japan
[*]duanni@umail.ucsb.edu

Abstract: For the first time, an ultra-compact integrated isolator without use of permanent magnets is designed and fabricated by bonding Ce:YIG on a silicon microring. Record isolation of 32dB and low 2.3dB excess loss were achieved.
OCIS codes: (230.3240) Isolators; (130.3120) Integrated optics devices; (230.3810) Magneto-optic systems.

1. Introduction

Optical isolators are an important, but challenging device to integrate on Si or III-V platforms in order to prevent undesired reflections from a laser cavity. Integrated optical isolators have largely relied on the nonreciprocal phase shift (NRPS) obtained by applying a magnetic field transverse to an asymmetric waveguide that is partially comprised of a magneto-optic material, like the cerium substituted yttrium iron garnet (Ce:YiG).

These devices are based on either unbalanced Mach-Zehnder interferometer (MZI) [1], or microring architecture [2]. To date, there have been several demonstrations of optical isolation on silicon using wafer bonding [3] or pulsed laser deposition [4]. However, several crucial issues must be addressed before isolators can be implemented in a photonic integrated circuit (PIC). One issue is that magneto-optic devices typically have a large insertion loss, which is related to the large footprint of MZI based isolators. A second issue is the use of a permanent magnet that is required to apply a static magnetic field close to the magneto-optic waveguides. This can cause problems in the eventual packaging of the PIC.

In this work, we address both of these issues by fabricating an ultra-compact microring based isolator with a current induced magnetic field that is directly integrated on chip. By achieving near-critical coupling to a 35μm radius ring, we demonstrate 32dB of isolation for the TM mode with an on-chip loss of 2.3dB at 1555nm.

2. Design and Simulation

The device is made up of an all-pass microring-based filter that is critically coupled to a straight waveguide, as schematically shown in Fig. 1.
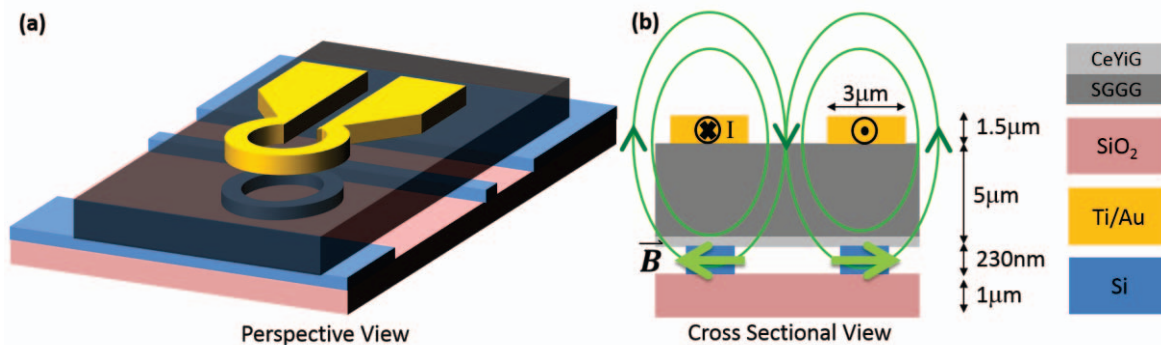

Figure 1: (a) 3-D view of the microring optical isolator and (b) device cross-section.

Both the microring and the bus waveguide are made of silicon (refractive index n_{Si}=3.44) with an air cladding (n_{Air}=1). A Ce:YIG layer (n_{CeYIG}=2.22), which was previously grown on a substituted gadolinium gallium garnet (SGGG, n_{SGGG}=1.97) substrate, is bonded over the silicon layer. All materials are low loss at λ=1550nm, with the exception of the Ce:YiG which has a propagation loss of 60dB/cm.

On top of the SGGG substrate, a metal wire in shape of a ring is designed to electrically induce a radial magnetic field (B in Fig. 1b). By applying such a field, the phase constant of the clockwise (CW) and the counter-clockwise (CCW) TM modes are different and the NRPS between them is achieved. The resonance wavelength split is estimated as $\Delta\lambda = (\Delta\beta \cdot \lambda)/ \beta_g$, where $\Delta\beta$ is the NRPS and β_g is the average group constant with respect to the two

directions. In order to maximize Δλ and the isolation, the waveguide cross-section and the Ce:YIG thickness have been optimized. For the simulation, the Faraday rotation θ of Ce:YIG is assumed to be -4500°/cm. The mode analysis is performed through a nonreciprocal mode solver based on the finite element method [5] and the results are shown in Fig. 2a. Because the bonding is achieved by O_2 plasma activation, a thin oxide spacer layer of 10nm is assumed between the Ce:YIG and the Si waveguide. The maximum resonance wavelength split (RWS) is obtained for a 215nm thick by 600nm wide silicon waveguide, and a 400nm thick Ce:YIG layer.

For those values, the maximum of the field is located close to the Ce:YIG/SiO$_2$/Si interfaces. For this reason, a larger bend radius of 35 µm and a thicker silicon waveguide are preferred (i.e., 230nm) in order to keep the mode better confined and reduce bend loss. In Fig. 2b, the degradation of the NRPS with respect to the oxide layer thickness is reported for three Faraday rotation values. As it is shown, a small increment in the oxide layer thickness strong reduces the nonreciprocal effect. For the proposed device, the critical power coupling coefficient K is about 11.68 %, which corresponds to a gap of about 245 nm. The critical coupling condition is crucial for microring-based systems because it is related to the ring-waveguide distance, which is difficult to be experimentally controlled with high accuracy [6]. Due to the large propagation loss in the Ce:YIG, the coupling condition is less strict and a variation up to 15% from the optimum gap can still guarantee an isolation higher than 20 dB, as shown in Fig. 2c.
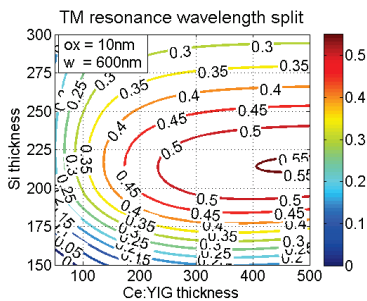
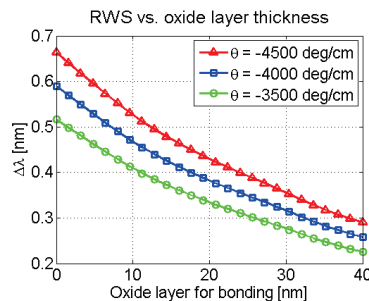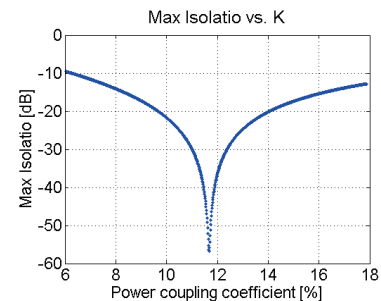| Figure 2 (a) Resonance wavelength splitting with respect to Si and Ce:YIG thicknesses	Figure 2 (b) RWS degradation with respect to the oxide layer thickness	Figure 2 (c) Isolation as a function of the power coupling coefficient

3. Fabrication and Characterization

Silicon waveguides are patterned on a 230 nm thick SOI wafer using 248 nm DUV lithography, and then dry etched. A 400 nm thick single crystal Ce:YIG layer was grown on a 300 µm thick SGGG substrate, and then diced into 3.5 mm × 10mm dies. Following an O_2 plasma activation of both the garnet and silicon surfaces, the Ce:YiG die is directly bonded onto the Si waveguides. The resulting bond is annealed at 200 °C for 6 hours under 3 MPa of pressure. Next, 1 µm of SiO$_2$ is sputtered to serve as an upper cladding, as well as protect the exposed Si waveguides that are not covered by the bonded die. Using a mechanical lapping technique, the SGGG substrate on the bonded die is thinned down from 300 µm to ~ 5 µm. Finally, 1.5 µm thick Ti/Au metal is patterned onto the back of the SGGG substrate using i-line lithography and subsequent metal liftoff. The width of the metal wires are designed to be 3 µm and the contact pads are 150 µm × 150µm. The fabricated devices are shown below in Fig. 3.
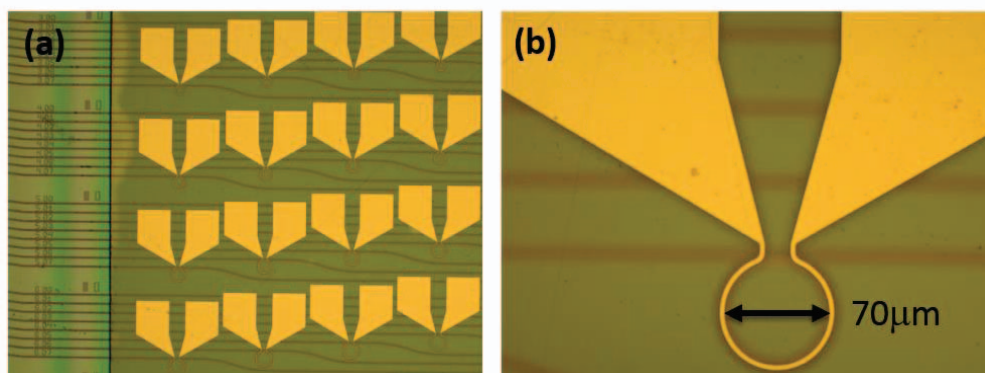
Figure 3: Optical micrographs of the fabricated device showing (a) splits of isolator geometries and (b) a single microring isolator.

We characterize the isolator by injecting light from a tunable laser source through a polarization maintaining (PM) fiber that is aligned to the TM mode of the waveguide. We align a single mode fiber at the output and observe the power of the transmitted light as the tunable laser is swept from 1500nm to 1570nm. We then inject a current through the contacts in order to induce a radial magnetic field with respect to the microring. To observe the

resonance wavelength shift, we reverse the direction of the current to flip the direction of the magnetic field, which is equivalent to switching the propagation direction of light. We extract the isolation of the device by measuring the extinction ratio between the two spectra at the resonance frequency. We obtain 32dB of isolation near 1555.26nm, using 80mA of current, for which we observe a nonreciprocal wavelength split of 0.16 nm as shown in Fig. 4a. We also flipped the direction of the light and measured the same isolation and loss.
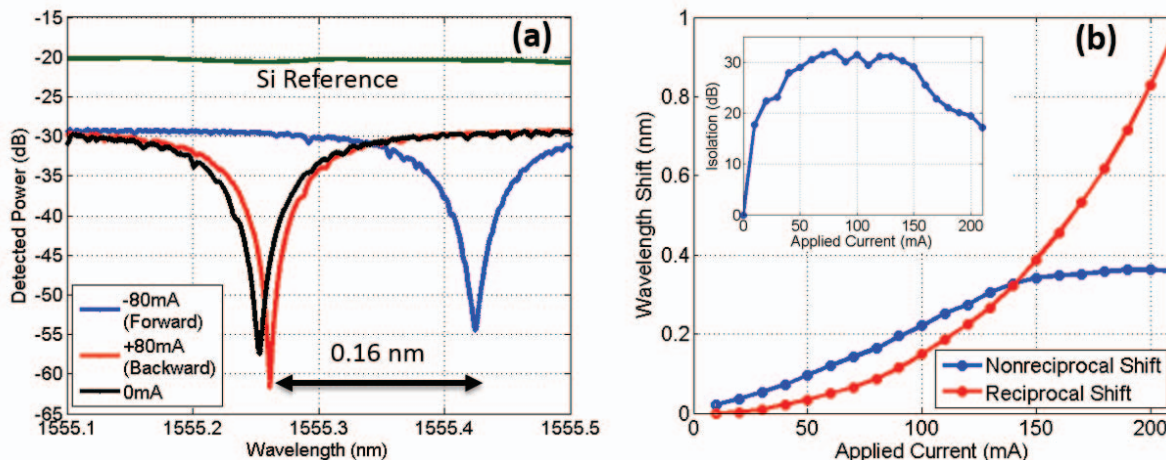

Figure 4: (a) Measured spectra with +/- 80mA of applied current. (b) Wavelength shift and isolation (inset) versus applied current.

We also notice a thermally induced redshift with quadratic dependence on the applied current (Joule heating effect), which is denoted as the reciprocal shift in Fig. 4b. One can imagine the black curve in Fig. 4a moving towards the right due to heating from the applied current. The magneto-optic nonreciprocal wavelength split operates on top of this redshift, resulting in the split between the forward (CW) and backward (CCW) spectra in Fig. 4a. We do not expect a change in temperature due to the change in sign of the current. The nonreciprocal wavelength split is roughly linear with applied current (also magnetic field) until it saturates at 0.35nm for 150mA of applied current, which confirm that the magnetization in the Ce:YiG has saturated. This value is smaller than the simulated one of 0.52 nm, because of the temperature dependence of Faraday rotation in Ce:YiG [7]. Moreover, a thicker oxide spacer and incomplete coverage of the metal wire around the ring also reduce the maximum reachable value. A further increase in current results in thermal tuning of the device, although the isolation drops as the device strays from critical coupling, as pictured in the inset of Fig. 4b.

The measured excess loss compared to a silicon reference waveguide is 10dB in Fig. 4a, of which a simulated 1.2dB is from scattering at the interfaces between the silica clad waveguide and Ce:YiG covered waveguide, and the remaining 8.8dB is attributed to absorption in the Ce:YiG, as confirmed by the simulations. This measured loss is large because the length of the Ce:YiG covered bus waveguide (3.5mm) is much longer than the diameter of the microring isolator (i.e., 70μm). Due to the need to place splits on mask, there is the equivalent length of eight isolators, including the width of the metal contact pads, across a single bus waveguide. Therefore, the excess loss of a single isolator based on these cutback calculations is (1.2 + 8.8/8) = 2.3dB.

4. Conclusion

An optical isolator is demonstrated by bonding Ce:YiG to a near-critically coupled silicon microring, and depositing a metal wire on the backside of the lapped bonded die. The metal simultaneously serves as an electromagnet as well as a thermal tuner for the ring. Using this novel approach, a record 32dB of isolation with 2.3dB of excess loss is achieved in an ultra-compact ring with 35μm radius.

References
[1] Y. Shoji and T. Mizumoto, "Magneto-optical non-reciprocal devices in silicon photonics," Sci. Tech. Adv. Mater. **15**, 014602 (2014).
[2] N. Kono, et al. "Nonreciprocal microresonators for the miniaturization of optical waveguide isolators," Opt. Express **15**, 7737–7751 (2007).
[3] M.-C. Tien, et al. "Silicon ring isolators with bonded nonreciprocal magneto-optic garnets," Opt. Express **19**, 11740-11745 (2011).
[4] L. Bi, et al. "On-chip optical isolation in monolithically integrated non-reciprocal optical resonators," Nat. Photon.**5**, 758-762 (2011).
[5] P. Pintus, "Accurate vectorial finite element mode solver for magneto-optic and anisotropic waveguides," Opt. Express **22**, 15737-15756 (2011).
[6] P. Pintus, et al. "Design of magneto-optical ring isolator on SOI based on the finite-element method," IEEE Photon. Technol. Lett **23**, 1670-1672 (2011).
[7] K. Furuya, et al. "Demonstration of an athermal waveguide optical isolator on silicon platform," 41st European Conference on Optical Communication (ECOC 2015).